UNCECOMP 2015
1st ECCOMAS Thematic Conference on
Uncertainty Quantification in Computational Sciences and Engineering
M. Papadrakakis, V. Papadopoulos, G. Stefanou (eds.)
Crete Island, Greece, 25–27 May 2015

AN EFFICIENT MESHLESS SOLUTION FOR THE FOKKER-PLANCK-KOLMOGOROV EQUATIONS OF PROBABILISTIC ELASTOPLASTICITY

Konstantinos Karapiperis[1], **Kallol Sett**[2] **and Boris Jeremić**[1]

[1]Department of Civil and Environmental Engineering, University of California, Davis
1 Shields Avenue, Davis, CA
e-mail: {kkarapiperis, jeremic}@ucdavis.edu

[2] Department of Civil, Structural and Environmental Engineering University at Buffalo, NY
12 Capen Hall, Buffalo, NY
e-mail: kallolse@buffalo.edu

Keywords: Fokker-Planck Equation, Elastoplasticity, Radial Basis Functions, Collocation, Galerkin

Abstract. *This paper describes the application of a numerical method for the solution of the nonlinear Fokker-Planck-Kolmogorov (FPK) equations of Probabilistic Elastoplasticity. We employ both a collocation and a Galerkin approach that utilize radial basis functions (RBFs) of various types, while time integration is achieved with the Crank-Nicolson scheme. The efficiency of the solution is demonstrated through simple linear elastic and elastic-perfectly plastic examples of various dimensionalities. In addition, we briefly address the accuracy and stability of the method with respect to the choice of RBF and the associated shape parameter. Finally, we provide a comparison with conventional solutions of the FPK equation to indicate the superiority of the approach.*

1 INTRODUCTION

Deterministic elastoplasticity has seen considerable advances during the last decades and advanced constitutive models are now able to capture the most inctricate aspects of material behaviour. However, most materials in nature are heterogeneous and thus inherently uncertain, which renders the treatment of uncertainty in this framework a necessity. Calibrating the components (elasticity, yield function, flow rule) of such a model by simply taking the mean of an experimental data set leads to a poor prediction of the actual response of a system. So far most of the available approaches regarding the modeling of stochastic irreversible behaviour has been based on Monte Carlo methods [1, 2]. The first attempt to propagate the uncertainties through elastoplastic constitutive equations was made by Anders and Hori, [3] who relied on a bounding media analysis. Later, Jeremić et al., [4, 5] developed a second-order exact E-L form of the Fokker-Planck-Kolmogorov (FPK) equation for the general elastoplastic constitutive rate equation. Finally, Rosić and Matthies, [6] presented the variational theory behind the mixed-hardening stochastic plasticity problem along with stochastic versions of the relevant established computational algorithms.

In this work, we deal with the FPK approach for stochastic plasticity. Its numerical solution is known to be computationally demanding especially in high dimensionalities and a number of solution procedures have been applied in the past. Traditionally it has been solved using the finite difference or finite element method [7, 8, 9], while a few researchers have also applied the path integration method [10, 11] as well as a multiscale finite element approach [12]. Only lately researchers have used a radial basis function (RBF) approach [13, 14] as well as a hybrid spectral-finite difference method [15]. Especially for high dimensional problems, researchers have combined sparse grid quadrature with several of the above techniques [16].

This work is divided into a theoretical part, where the basic features of FPK-based probabilistic elastoplasticity are laid out and a numerical part, which involves the application of a meshfree RBF-based solution, including convergence and basic stability analysis. Results of probabilistic constitutive integration are presented and verified against pertinent Monte Carlo simulations (MCS).

2 THEORY

The incremental form of spatial-average elastoplastic constitutive equation in 3D may be written as

$$\frac{d\sigma_{ij}(x_t,t)}{dt} = D_{ijkl}(x_t,t)\frac{d\epsilon_{kl}(x_t,t)}{dt} \tag{1}$$

where D_{ijkl} is the continuum stiffness tensor which can be either elastic or elasto-plastic

$$D_{ijkl} = \begin{cases} D^{el}_{ijkl} & ;f<0 \vee (f=0 \wedge df<0) \\ D^{el}_{ijkl} - \dfrac{D^{el}_{ijmn}\frac{\partial U}{\partial \sigma_{mn}}\frac{\partial f}{\partial \sigma_{pq}}D^{el}_{pqkl}}{\frac{\partial f}{\partial \sigma_{rs}}D^{el}_{rstu}\frac{\partial U}{\partial \sigma_{tu}} - \frac{\partial f}{\partial q_*}r_*} & ;f=0 \wedge df<0 \end{cases} \tag{2}$$

where D^{el}_{ijkl} is the elastic stiffness tensor, f is the yield function, which is a function of stress σ_{ij} and internal variables q_* and U is the plastic potential function. In its most general form, the incremental constitutive equation takes the form

$$\frac{d\sigma_{ij}(x_t,t)}{dt} = \beta_{ijkl}(\sigma_{ij}, D_{ijkl}, q_*, r_*; x_t, t)\frac{d\epsilon_{kl}(x_t,t)}{dt} \tag{3}$$

or

$$\frac{d\sigma_{ij}(x_t,t)}{dt} = \eta_{ijkl}(\sigma_{ij}, D_{ijkl}, \epsilon_{kl}(x_t,t)q_*, r_*; x_t, t) \tag{4}$$

where the stochasticity of the operator β is induced by the stochasticity of D_{ijkl}, q_*, r_*. This renders the above equation a linear/non-linear ordinary differential equation with stochastic coefficients. Similarly randomness in the forcing term (ϵ_{kl}) results in a linear/non-linear ordinary differential equation with stochastic forcing. Combining the two cases yields, of course, a linear/non-linear ordinary differential equation with stochastic coefficients and stochastic forcing. Using the Eulerian-Lagrangian form of the FPK equation [17], the above equation takes the following form in the probability density space

$$\begin{aligned}
\frac{\partial P(\sigma_{ij}(t),t)}{\partial t} &= -\frac{\partial}{\partial \sigma_{mn}}\left[\{\langle \eta_{mn}(\sigma_{mn}(t), D_{mnrs}, \epsilon_{rs}(t))\rangle\right. \\
&+ \int_0^t d\tau Cov_0\left[\frac{\partial \eta_{mn}(\sigma_{mn}(t), D_{mnrs}, \epsilon_{rs}(t))}{\partial \sigma_{ab}};\right. \\
&\left.\left. \eta_{ab}(\sigma_{ab}(t-\tau), D_{abcd}, \epsilon_{cd}(t-\tau))\right]\right\} P(\sigma_{ij}(t),t)\Big] \\
&+ \frac{\partial^2}{\partial \sigma_{mn}\partial \sigma_{ab}}\left[\int_0^t d\tau Cov_0\left[\eta_{mn}(\sigma_{mn}(t), D_{mnrs}, \epsilon_{rs}(t));\right.\right. \\
&\left.\left. \eta_{ab}(\sigma_{ab}(t-\tau), D_{abcd}, \epsilon_{cd}(t-\tau))\right] P(\sigma_{ij}(t),t)\right]
\end{aligned} \tag{5}$$

where $P(\sigma(t),t)$ is the probability density of stress, $\langle\cdot\rangle$ is the expectation operator, $Cov_0[\cdot]$ is the time-ordered covariance operator and η_{ij} is a generalized random operator tensor (see previous equation). Details of this derivation can be found in [4]. The above equation is equivalent to the following simplified version:

$$\frac{\partial P(\sigma_{ij}(t),t)}{\partial t} = \frac{\partial}{\partial \sigma_{mn}}\left[N_{(1)_{mn}} P(\sigma_{ij},t) - \frac{\partial}{\partial \sigma_{ab}}\{N_{(2)_{mnab}} P(\sigma_{ij},t)\}\right] \tag{6}$$

where $N_{(1)}$ and $N_{(2)}$ are appropriate advection and diffusion coefficients respectively. With appropriate initial and boundary conditions, and given the second-order statistics of material properties,the equation can be solved with second-order accuracy. The advection and diffusion coefficients are particular to the constitutive model.

To introduce the uncertainty in the probabilistic yielding we apply the probability of yielding as a weight factor in the plastic corrector, denoted by D^{pl}_{ijkl}. This allows us to derive the stochastic elastoplastic stiffness tensor:

$$D_{ijkl} = D^{el}_{ijkl} - \Phi D^{pl}_{ijkl} \tag{7}$$

where e.g for J_2 plasticity:

$$\Phi = P[\sigma_y \leq \sqrt{3J_2}] \tag{8}$$

Introducing Eq. (7) to Eq. (6) we can derive the general form of the elastoplastic advection and diffusion coefficients as follows:

$$\begin{aligned}
N^{\sigma^{ep}}_{(1)_{mn}} &= \langle (D^{el}_{mnrs} - \Phi D^{pl}_{mnrs})\dot{\epsilon}_{rs}\rangle \\
&+ \int_0^\tau d\tau Cov_0\left[\frac{\partial}{\partial \sigma_{ab}}\{D^{el}_{mnrs} - \Phi D^{pl}_{mnrs}\}|_t\ \dot{\epsilon}_{rs}; -\Phi D^{pl}_{mnab}|_{t-\tau}\ \dot{\epsilon}_{ab}\right]
\end{aligned} \tag{9}$$

Assuming a linear elastic stiffness tensor the above simplifies to

$$\begin{aligned} N^{\sigma^{ep}}_{(1)_{mn}} &= (\langle D^{el}_{mnrs}\rangle - \langle \Phi D^{pl}_{mnrs}\rangle)\dot{\epsilon}_{rs} \\ &+ \int_0^\tau d\tau Cov_0 \left[-\frac{\partial}{\partial \sigma_{ab}} \{\Phi D^{pl}_{mnrs}\}|_t \ \dot{\epsilon}_{rs}; (D^{el}_{mnab} - \Phi D^{pl}_{mnab})|_{t-\tau} \ \dot{\epsilon}_{ab} \right] \end{aligned} \tag{10}$$

For the elastoplastic diffusion coefficient we have:

$$N^{\sigma^{ep}}_{(2)_{mnab}} = \int_0^\tau d\tau Cov_0 \left[(D^{el}_{mnrs} - \Phi D^{pl}_{mnrs})|_t \ \dot{\epsilon}_{rs}; (D^{el}_{abcd} - \Phi D^{pl}_{abcd})|_{t-\tau} \ \dot{\epsilon}_{cd} \right] \tag{11}$$

It is important for the accuracy of the method that the evolving correlation structure be captured to a satisfactory accuracy. For this reason, Monte Carlo simulations need to be employed in order to construct an analytical function describing the evolving correlation kernel for a specific type of elastoplastic model.

Finally, when hardening is described by a vector internal variable $\mathbf{q}$, the evolution of the latter is captured through a coupled FPK equation, in which the drift and diffusion coefficients are given by:

$$N^{IV}_{(1)_i} = \langle \Phi L r_i(\sigma, \mathbf{q}, t)\rangle + \int_0^t d\tau Cov_0 \left[\frac{\partial}{\partial q_j} \{\Phi L r_i\}; \{\Phi L r_j\} \right] \tag{12}$$

$$N^{IV}_{(2)_{ij}} = \int_0^t d\tau Cov_0 \left[\Phi L r_i; \Phi L r_j \right] \tag{13}$$

where L is the loading index:

$$L = \frac{\frac{\partial f}{\partial \sigma_{rs}} D^{el}_{ijrs} \dot{\epsilon_{ij}}}{\frac{\partial U}{\partial \sigma_{ab}} D^{el}_{abcd} \frac{\partial f}{\partial \sigma_{cd}} - \frac{\partial f}{\partial q_n} r_n} \tag{14}$$

3 NUMERICAL METHOD

An RBF approximant depends on the distance to a center point $\mathbf{x}_j$ and is usually of the form $\phi(\|\mathbf{x} - \mathbf{x}_j\|)$. Some commonly used infinitely smooth RBFs are given in Table 1 [18].

RBF	$\phi(\|\mathbf{x} - \mathbf{x}_j\|)$
Gaussian	$e^{-\epsilon^2 \cdot (\mathbf{x} - \mathbf{x}_j)^2}$
Multiquadric	$\sqrt{(\mathbf{x} - \mathbf{x}_j)^2 + \epsilon^2}$
Inverse Multiquadric	$\frac{1}{\sqrt{(\mathbf{x} - \mathbf{x}_j)^2 + \epsilon^2}}$

Table 1: Some common RBF interpolating functions

It is considered a meshless method, since it only requires a set of scattered nodes which are located in the domain of interest. An RBF interpolant is a linear combination of RBFs centered at the aforementioned points:

$$u(\mathbf{x}) = \sum_{i=1}^{N} u_i \phi(\|\mathbf{x} - \mathbf{x}_i\|) \tag{15}$$

where $\|\cdot\|$ denotes the Euclidian distance between two points and u_i appropriate coefficients to be determined. The latter may be achieved by collocation, in which case the residual is minimized at as many spatial points as possible. Straight or asymmetric collocation involves collocating with boundary data at the boundary points and with the PDE at the interior points, which is what is used herein. This may sometimes lead to a singular coefficient matrix, which is why some researchers have introduced symmetric collocation approaches to assure non-singularity of the coefficient matrix. A more detailed study of different radial basis functions and collocation methods can be found in [18]. Apart from collocation, we will investigate a Bubnov-Galerkin projection approach to a trial space same as the test space.

For the purpose of our problem, let Ω, $\partial\Omega$ be the set of interior points and boundary points of the domain of interest respectively. Then the constitutive equation may be described by:

$$\frac{\partial P(\sigma,t)}{\partial t} = \mathcal{L}(P(\sigma,t) \qquad \text{in } \Omega \tag{16}$$

$$\mathcal{B}(P(\sigma,t) = 0 \qquad \text{in } \partial\Omega \tag{17}$$

where $\mathcal{L}$ is a linear (elastic):

$$\mathcal{L}^{el}(\cdot) = -N^{el}_{(1)}\frac{\partial(\cdot)}{\partial\sigma} + N^{el}_{(2)}\frac{\partial^2(\cdot)}{\partial\sigma^2} \tag{18}$$

or nonlinear (elastoplastic) differential operator:

$$\mathcal{L}^{eq}(\cdot) = -N^{eq}_{(1)}\frac{\partial(\cdot)}{\partial\sigma} - (\cdot)\frac{\partial N^{eq}_{(1)}}{\partial\sigma} + N^{eq}_{(2)}\frac{\partial^2(\cdot)}{\partial\sigma^2} + 2\frac{\partial N^{eq}_{(2)}}{\partial\sigma}\frac{\partial(\cdot)}{\partial\sigma} + \frac{\partial^2 N^{eq}_{(2)}}{\partial\sigma^2}(\cdot) \tag{19}$$

and $\mathcal{B}$ is the boundary condition operator:

$$\mathcal{B}(\cdot) = N^{eq}_{(1)}(\cdot) - \frac{\partial}{\partial\sigma}[N^{eq}_{(2)}(\cdot)] \tag{20}$$

derived from the application of reflective boundaries, necessary to enforce a zero probability current ζ.

Taking the RBF interpolants over the domain grid, we may approximate the probability density as:

$$P(\sigma,t) = \sum_{i=1}^{N} a_i(t)\phi(\|\sigma-\sigma_i\|_2) \tag{21}$$

where ϕ denotes the radial basis functions and a_i appropriate coefficients to be determined. Then, following the notation of [19], we may write:

$$\mathcal{L}(P(\sigma_i,t)) = \sum_{j=1}^{N} a_j(t)\mathcal{L}(\phi(\|\sigma_i-\sigma_j\|_2)) \qquad i=1,\ldots,N_I \tag{22}$$

$$\mathcal{B}(P(\sigma_i,t)) = \sum_{j=1}^{N} a_j(t)\mathcal{B}(\phi(\|\sigma_i-\sigma_j\|_2)) \qquad i=N_I+1,\ldots,N \tag{23}$$

where $N_I, N_B = N - N_I$ denote the interior and boundary points. It is evident that spatial derivatives are determined by simply differentiating the RBFs. In order to determine the grid, boundaries ($\partial\Omega$) are covered in an equispaced fashion and a spacing algorithm (e.g Greedy

algorithm) may be employed for the interior domain (Ω). The use of Gaussian kernels is a good choice for this particular application, since we expect the solution to remain gaussian in the elastic regime and approximately skewed gaussian in the elastoplastic regime.

The Crank-Nicolson scheme is employed for time integration due to its unconditional stability:

$$\frac{\partial P(\sigma,t)}{\partial t} = \frac{1}{2}\Big(\frac{P(\sigma,t+\frac{\Delta t}{2}) - P(\sigma,t)}{\frac{\Delta t}{2}} + \frac{P(\sigma,t+\Delta t) - P(\sigma,t+\frac{\Delta t}{2})}{\frac{\Delta t}{2}}\Big) \tag{24}$$

3.1 Linear Elastic Problem

Specializing the problem to the case of linear elasticity yields:

$$\begin{aligned} & P(\sigma,t^{n+1}) - \frac{\Delta t}{2}\Big(- N^{el}_{(1)_m}\frac{\partial P(\sigma,t^{n+1})}{\partial \sigma_m} + N^{el}_{(2)_{mn}}\frac{\partial^2 P(\sigma,t^{n+1})}{\partial \sigma_m \sigma_n}\Big) \\ = \;& P(\sigma,t^{n}) + \frac{\Delta t}{2}\Big(- N^{el}_{(1)_m}\frac{\partial P(\sigma,t^{n})}{\partial \sigma_m} + N^{el}_{(2)_{mn}}\frac{\partial^2 P(\sigma,t^{n})}{\partial \sigma_m \sigma_n}\Big) \end{aligned} \tag{25}$$

where summation is implied over the repeated indices m, n associated with the dimensionality of the problem. Looking at the solution in a point $\sigma_i = \{\sigma_1, \ldots, \sigma_m\}_i$ in the discretized space, we have:

$$\begin{aligned} & \sum_{j=1}^{N} a_j^{n+1}\phi_{ij} - \frac{\Delta t}{2}\Big(- N^{el}_{(1)_m}\sum_{j=1}^{N} a_j^{n+1}\frac{\partial \phi_{ij}}{\partial \sigma_m} + N^{el}_{(2)_{mn}}\sum_{j=1}^{N} a_j^{n+1}\frac{\partial \phi^2_{ij}}{\partial \sigma_m \sigma_n}\Big) \\ = \;& \sum_{j=1}^{N} a_j^{n}\phi_{ij} + \frac{\Delta t}{2}\Big(- N^{el}_{(1)_m}\sum_{j=1}^{N} a_j^{n}\frac{\partial \phi_{ij}}{\partial \sigma_m} + N^{el}_{(2)_{mn}}\sum_{j=1}^{N} a_j^{n}\frac{\partial \phi^2_{ij}}{\partial \sigma_m \sigma_n}\Big) \end{aligned} \tag{26}$$

where $\phi_{ij} = \phi(||(\sigma_i - \sigma_j)||)$.

Notice that the summation associated with the RBF representation is stated explicitly.

Direct collocation renders the last equation equivalent to:

$$T^L_{ij} a_j^{n+1} = T^R_{ij} a_j^n \tag{27}$$

where

$$T^L_{ij} = \phi_{ij} - \frac{\Delta t}{2}\Big(- N^{el}_{(1)_m}\frac{\partial \phi_{ij}}{\partial \sigma_m} + N^{el}_{(2)_{mn}}\frac{\partial^2 \phi_{ij}}{\partial \sigma_m \sigma_n}\Big) \tag{28}$$

$$T^R_{ij} = \phi_{ij} + \frac{\Delta t}{2}\Big(- N^{el}_{(1)_m}\frac{\partial \phi_{ij}}{\partial \sigma_m} + N^{el}_{(2)_{mn}}\frac{\partial^2 \phi_{ij}}{\partial \sigma_m \sigma_n}\Big) \tag{29}$$

Similarly the boundary conditions of Eq. (23) can be written as:

$$B_{ij} a_j^{n+1} = 0 \tag{30}$$

where according to Eq. (20)

$$B_{ij} = \sum_m \Big(N^{el}_{(1)_m}\phi_{ij} - N^{el}_{(2)_{mn}}\frac{\partial \phi_{ij}}{\partial \sigma_n}\Big) \tag{31}$$

Therefore, the system of equations to be solved becomes:

$$\left[\begin{array}{c} \mathbf{B} \\ --- \\ \mathbf{T^L} \end{array}\right] \left\{a^{n+1}\right\} = \left[\begin{array}{c} \mathbf{0} \\ --- \\ \mathbf{T^R} \end{array}\right] \{a^n\} \tag{32}$$

Note that the non-periodic nature of the solution domain (in contrast to the Fourier approach) necessitates the explicit imposition of the reflective boundary conditions as shown above. Alternatively one may apply a **Galerkin projection** rather than direct collocation. Thus, the error of the representation is minimized in an average sense rather than in discrete points. In this sense, we can easily derive the following weak form of Eq. (26) as:

$$\begin{aligned} &\sum_{j=1}^{N} a_j^{n+1} \int_\Omega \left[\phi_j - \frac{\Delta t}{2}\Big(- N^{el}_{(1)_m} \frac{\partial \phi_j}{\partial \sigma_m} + N^{el}_{(2)_{mn}} \frac{\partial \phi_j^2}{\partial \sigma_m \sigma_n}\Big)\right] \times \phi_i d\Omega \\ = &\sum_{j=1}^{N} a_j^{n} \int_\Omega \left[\phi_j + \frac{\Delta t}{2}\Big(- N^{el}_{(1)_m} \frac{\partial \phi_j}{\partial \sigma_m} + N^{el}_{(2)_{mn}} \frac{\partial \phi_j^2}{\partial \sigma_m \sigma_n}\Big)\right] \times \phi_i d\Omega \end{aligned} \tag{33}$$

where $\phi_j = \phi(||\sigma - \sigma_j||)$ and $\phi_i = \phi(||\sigma_i - \sigma||)$.

Thus the Eq. (28), (29) analogue is derived as

$$T^L_{ij} = \int_\Omega \left[\phi_j - \frac{\Delta t}{2}\Big(- N^{el}_{(1)_m} \frac{\partial \phi_j}{\partial \sigma_m} + N^{el}_{(2)_{mn}} \frac{\partial \phi_j^2}{\partial \sigma_m \sigma_n}\Big)\right] \times \phi_i d\Omega \tag{34}$$

$$T^R_{ij} = \int_\Omega \left[\phi_j + \frac{\Delta t}{2}\Big(- N^{el}_{(1)_m} \frac{\partial \phi_j}{\partial \sigma_m} + N^{el}_{(2)_{mn}} \frac{\partial \phi_j^2}{\partial \sigma_m \sigma_n}\Big)\right] \times \phi_i d\Omega \tag{35}$$

Finally, the Eq. (31) analogue is derived as:

$$B_{ij} = \int_\Omega \left[\sum_m \left(N^{el}_{(1)_m} \phi_j - N^{el}_{(2)_{mn}} \frac{\partial \phi_j}{\partial \sigma_n}\right)\right] \times \phi_i d\Omega \tag{36}$$

3.2 Elastoplastic problem

Generalization to the nonlinear problem yields state dependent coefficients in Eq. (25), so that we get:

$$\begin{aligned} &P(\sigma, t^{n+1}) - \frac{\Delta t}{2}\Big[- \frac{\partial}{\partial \sigma_m}\Big(N^{eq}_{(1)_m}(\sigma) P(\sigma, t^{n+1})\Big) + \frac{\partial^2}{\partial \sigma_m \sigma_n}\Big(N^{eq}_{(2)_{mn}}(\sigma) P(\sigma, t^{n+1})\Big)\Big] \\ = \; &P(\sigma, t^{n}) + \frac{\Delta t}{2}\Big[- \frac{\partial}{\partial \sigma_m}\Big(N^{eq}_{(1)_m}(\sigma) P(\sigma, t^{n})\Big) + \frac{\partial^2}{\partial \sigma_m \sigma_n}\Big(N^{eq}_{(2)_{mn}}(\sigma) P(\sigma, t^{n})\Big)\Big] \end{aligned} \tag{37}$$

After introducing the RBF discretization the resulting system of equations becomes:

$$\left\{\begin{array}{rcl} T^L_{ij} a_j^{n+1} &=& T^R_{ij} a_j^n \\ B_{ij} a_j^{n+1} &=& 0 \end{array}\right. \tag{38}$$

where according to **direct collocation**:

$$T^L_{ij} = \phi_{ij} - \frac{\Delta t}{2}\Big[- N^{eq}_{(1)_m}(\sigma_i) \frac{\partial \phi_{ij}}{\partial \sigma_m} - \frac{\partial N^{eq}_{(1)_m}}{\partial \sigma_m}\Big|_{\sigma=\sigma_i} \phi_{ij}$$

$$+N^{eq}_{(2)_{mn}}(\sigma_i)\frac{\partial^2\phi_{ij}}{\partial\sigma_m\sigma_n}+2\frac{\partial N^{eq}_{(2)_{mn}}}{\partial\sigma_m}\Big|_{\sigma=\sigma_i}\frac{\partial\phi_{ij}}{\partial\sigma_n}+\frac{\partial^2 N^{eq}_{(2)_{mn}}}{\partial\sigma_m\sigma_n}\Big|_{\sigma=\sigma_i}\phi_{ij}\Big] \quad (39)$$

$$T^R_{ij} = \phi_{ij}+\frac{\Delta t}{2}\Big[-N^{eq}_{(1)_m}(\sigma_i)\frac{\partial\phi_{ij}}{\partial\sigma_m}-\frac{\partial N^{eq}_{(1)_m}}{\partial\sigma_m}\Big|_{\sigma=\sigma_i}\phi_{ij}$$
$$+N^{eq}_{(2)_{mn}}(\sigma_i)\frac{\partial^2\phi_{ij}}{\partial\sigma_m\sigma_n}+2\frac{\partial N^{eq}_{(2)_{mn}}}{\partial\sigma_m}\Big|_{\sigma=\sigma_i}\frac{\partial\phi_{ij}}{\partial\sigma_n}+\frac{\partial^2 N^{eq}_{(2)_{mn}}}{\partial\sigma_m\sigma_n}\Big|_{\sigma=\sigma_i}\phi_{ij}\Big] \quad (40)$$

$$B_{ij} = \sum_m\Big(N^{eq}_{(1)_m}(\sigma_i)\phi_{ij}-N^{eq}_{(2)_{mn}}(\sigma_i)\frac{\partial\phi_{ij}}{\partial\sigma_n}-\frac{\partial N^{eq}_{(2)_{mn}}}{\partial\sigma_n}\Big|_{\sigma=\sigma_i}\phi_{ij}\Big) \quad (41)$$

or by employing **Galerkin projection**:

$$T^L_{ij} = \int_\Omega\Big[\phi_j-\frac{\Delta t}{2}\Big(-N^{eq}_{(1)_m}(\sigma_i)\frac{\partial\phi_j}{\partial\sigma_m}-\frac{\partial N^{eq}_{(1)_m}}{\partial\sigma_m}\Big|_{\sigma=\sigma_i}\phi_j$$
$$+N^{eq}_{(2)_{mn}}(\sigma_i)\frac{\partial^2\phi_j}{\partial\sigma_m\sigma_n}+2\frac{\partial N^{eq}_{(2)_{mn}}}{\partial\sigma_m}\Big|_{\sigma=\sigma_i}\frac{\partial\phi_j}{\partial\sigma_n}+\frac{\partial^2 N^{eq}_{(2)_{mn}}}{\partial\sigma_m\sigma_n}\Big|_{\sigma=\sigma_i}\phi_j\Big)\Big]\times\phi_i d\Omega \quad (42)$$

$$T^R_{ij} = \int_\Omega\Big[\phi_j+\frac{\Delta t}{2}\Big(-N^{eq}_{(1)_m}(\sigma_i)\frac{\partial\phi_j}{\partial\sigma_m}-\frac{\partial N^{eq}_{(1)_m}}{\partial\sigma_m}\Big|_{\sigma=\sigma_i}\phi_j$$
$$+N^{eq}_{(2)_{mn}}(\sigma_i)\frac{\partial^2\phi_j}{\partial\sigma_m\sigma_n}+2\frac{\partial N^{eq}_{(2)_{mn}}}{\partial\sigma_m}\Big|_{\sigma=\sigma_i}\frac{\partial\phi_j}{\partial\sigma_n}+\frac{\partial^2 N^{eq}_{(2)_{mn}}}{\partial\sigma_m\sigma_n}\Big|_{\sigma=\sigma_i}\phi_j\Big)\Big]\times\phi_i d\Omega \quad (43)$$

$$B_{ij} = \int_\Omega\Big[\sum_m\Big(N^{eq}_{(1)_m}(\sigma_i)\phi_{ij}-N^{eq}_{(2)_{mn}}(\sigma_i)\frac{\partial\phi_{ij}}{\partial\sigma_n}-\frac{\partial N^{eq}_{(2)_{mn}}}{\partial\sigma_n}\Big|_{\sigma=\sigma_i}\phi_{ij}\Big)\Big]\times\phi_i d\Omega \quad (44)$$

3.3 Results/Verification

In Figures 1,2 we provide results from 1D elastic-perfectly plastic simulations, which we verify against pertinent Monte Carlo simulations. Only a slight error can be identified in the transition region. To illustrate the applicability of the method to higher dimensions, Figure 3 shows a simulation in the case of plane strain elastic-perfectly plastic Mises material. Both the stress solution and the Mises yield criterion are depicted with 3-D probability contours.

3.4 Convergence/Stability of the method

The stability and accuracy of the method generally still remains a open problem in the literature. It is well known that it is generally susceptible to the Runge Phenomenon, in which the amplitude of the oscillations near the boundaries grows exponentially. When RBF centers cover a domain in a fairly uniform manner, the largest errors occur near the boundary [19]. Thus, different node-clustering techniques at the boundaries (e.g. Chebyshev grid) have been suggested to overcome this instability [20].

The accuracy of the method depends on the location of the centers with respect to the points where the interpolating functions are evaluated, which in general need not coincide. In addition, the value of the RBF shape parameter ϵ has been shown to play an important role. In general it needs to be chosen in such a way that the interpolation matrix remain relatively well-conditioned while keeping a satisfactory order of accuracy (theoretically spectral for Gaussian RBFs). As the basis functions become flatter, the accuracy increases but then the resulting system becomes ill-conditioned. Special techniques can be employed to lower the condition number $\kappa(\Phi)$ of the coefficient matrix and lead to stable computations with Gaussian RBFs [21, 22]. Fig. 4,5 portray

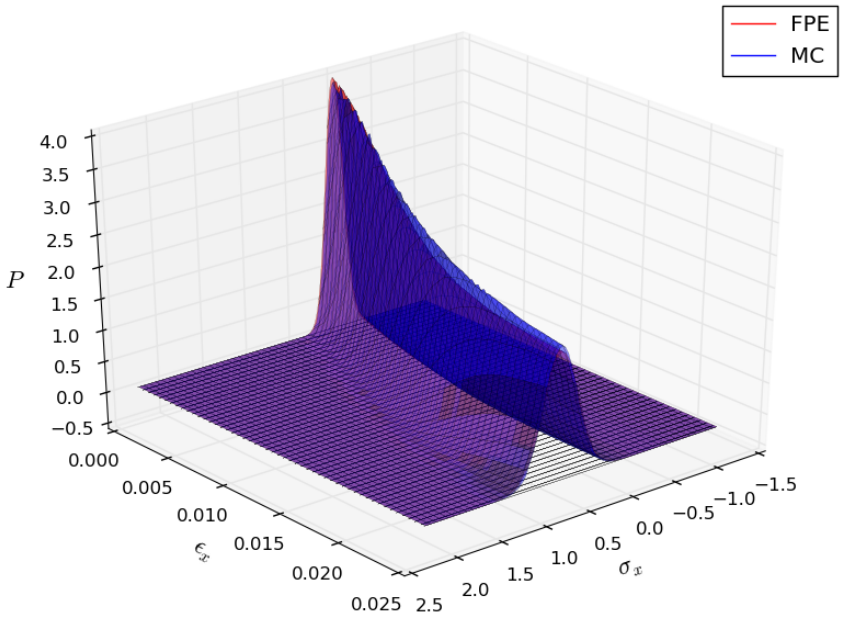

Figure 1: Verification of 1D elastic-perfectly plastic model using MCS in the case of high uncertainty in the yield stress.

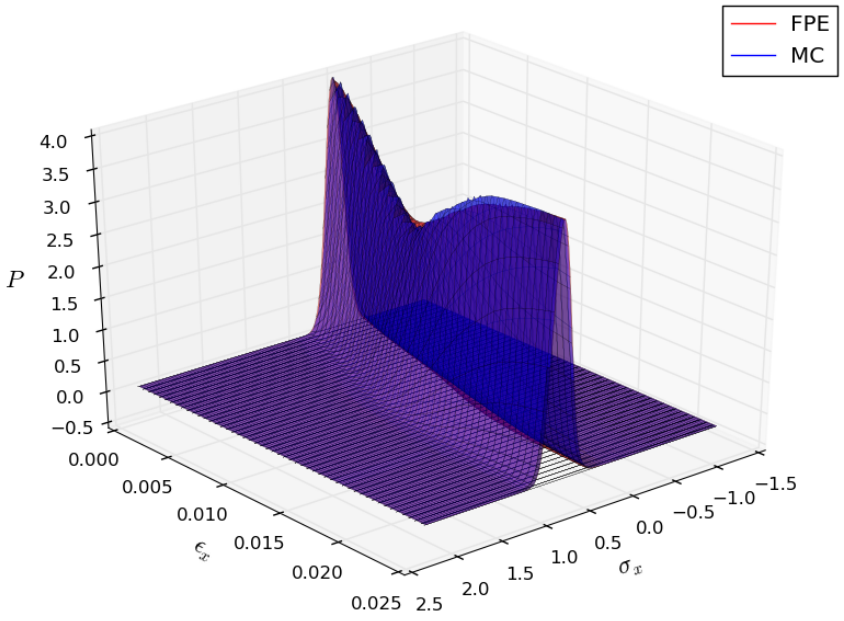

Figure 2: Verification of 1D elastic-perfectly plastic model using MCS in the case of low uncertainty in the yield stress.

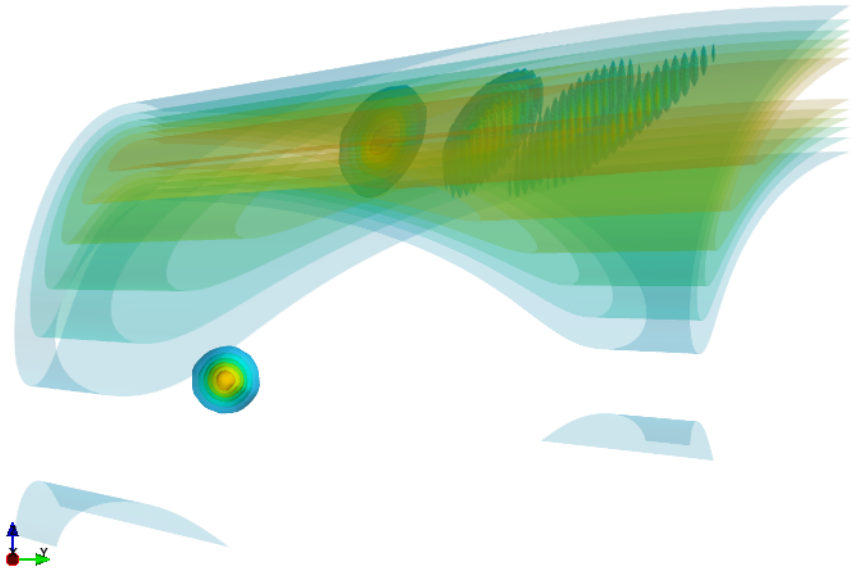

Figure 3: Plane strain Mises elastic-perfectly plastic simulation

the spatial convergence and stability properties of Gaussian and MQ RBFs in accordance with the above observations. In this work, the convergence rate is evaluated through the root mean square error:

$$E_{RMS} = \sqrt{\frac{1}{N}\sum_{i=1}^{N}(P_{ex}^{(i)} - P_{num}^{(i)})^2} \tag{45}$$

while the stability is evaluated by means of the condition number, namely the ratio of the largest to the smallest singular values of the coefficient matrix:

$$\kappa(\Phi) = \|\Phi^{-1}\| \cdot \|\Phi\| = \frac{\sigma_{max}}{\sigma_{min}} \tag{46}$$

It has been heuristically argued that ϵ should vary with the center location, thereby improving the condition number of the coefficient matrix [23]. Simple rules to advanced evolutionary optimization can been applied to assist the choice of the shape parameters.

Finally, the temporal convergence of the Crank-Nicolson scheme is shown in Fig. 6.

3.5 Comparison with other methods

To illustrate the efficiency of the method, we compare the root mean square error and the associated computational time for the meshless RBF method and for a forward finite difference - method of lines (MOL) scheme applied in a 1-D problem. Table 2 clearly indicates the superiority of the RBF solution, under the condition that the shape parameter is appropriately selected.

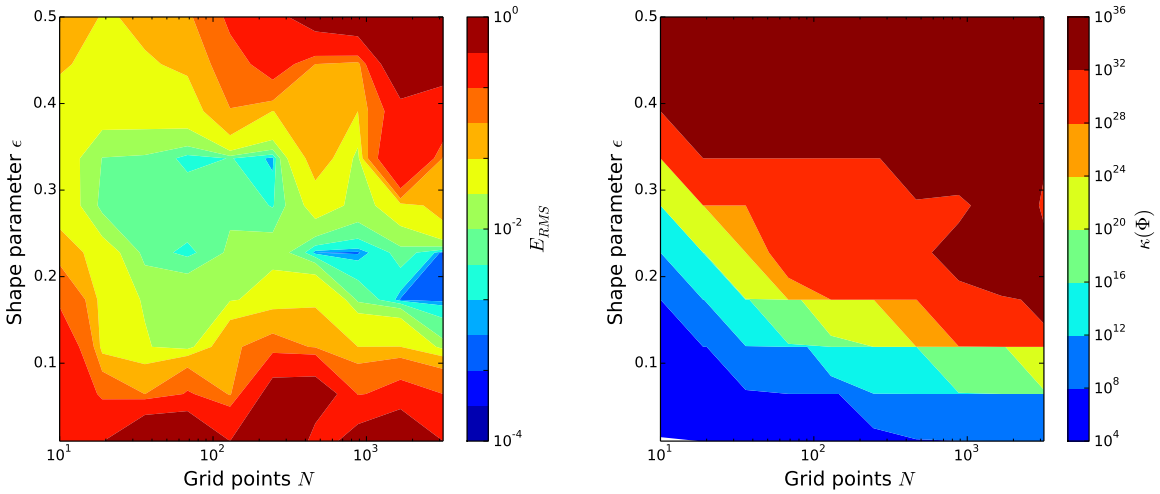

Figure 4: Convergence and stability map of multiquadratic basis function.

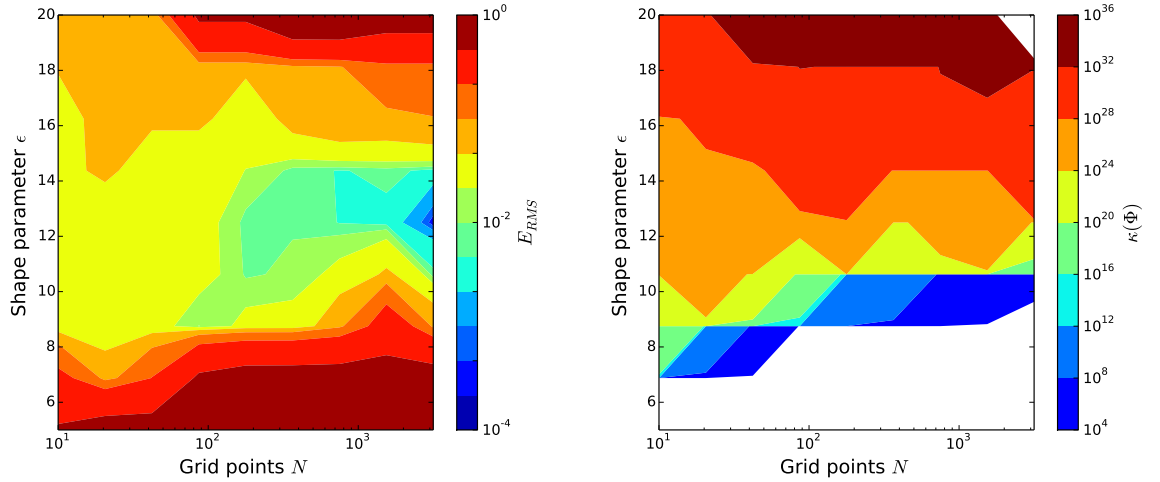

Figure 5: Convergence and stability map of Gaussian basis function.

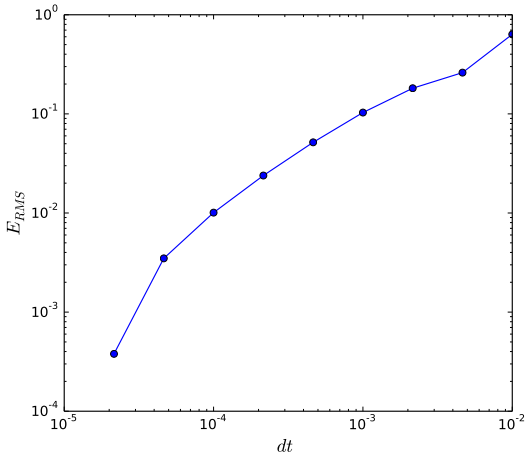

Figure 6: Temporal convergence for the Crank-Nicolson scheme.

Meshless RBF			Conventional FD		
Grid pts N	Avg. error E_{RMS}	Run time (s)	Grid pts N	Avg. error E_{RMS}	Run time (min)
100	0.1	0.5	5000	0.2	14
500	0.027	2.3	10000	0.017	112
1000	0.0051	4.5	20000	0.092	910

Table 2: Comparison of the efficiency of the meshless method with that of a conventional finite difference approach.

4 CONCLUSIONS

- Either through collocation or Galerkin projection, RBF methods are easy to implement and have low algorithmic complexity.
- Being meshless, they overcome the problem of generating a mesh over a potentially irregular domain in multiple dimensions.
- There is a trade-off between accuracy and stability, which requires the careful selection of the shape parameter.
- Under the optimal choice of shape parameter and for a nearly Gaussian problem, Gaussian RBF interpolation displays spectral convergence.
- The asymmetric interpolation matrix constructed by RBFs can be ill-conditioned, so that an appropriate preconditioner may be required to solve the resulting equations.

REFERENCES

[1] Fenton, Gordon A. and Griffiths, D. V., Bearing Capacity Prediction of Spatially Random $c - \phi$ Soil. *Canadian Geotechnical Journal*, Vol.40, p.54-65, 2003.

[2] Schueller G., Spanos P., Monte Carlo simulation. Balkema, Rotterdam, 2001.

[3] Anders, M. and Hori, M., Stochastic Finite Element Method for Elasto-Plastic Body. *Int. Journal for Numerical Methods in Engineering*, Vol.46 No.11, p.1897-1916, 1999.

[4] Jeremić, B., Sett, K. and Kavvas M.L, Probabilistic Elasto-Plasticity: Formulation in 1–D. *Acta Geotechnica*, Vo.2, No.3 p.197-210, 2007.

[5] Jeremić, B. and Sett, K., On Probabilistic Yielding of Materials. *Communications in Numerical Methods in Engineering*, Vol.25, No.3 p.291-300, 2009.

[6] Rosić, B. and Matthies, H., Variational Theory and Computations in Stochastic Plasticity, *Archives of Computational Methods in Engineering*, p.1-53, 2014

[7] Langley, R.S, A finite element method for the statistics of non-linear random vibrations, *Journal of Sound and Vibration*, Vol.101, No.1, p.41-54, 1985

[8] Langtangen, H., A General Numerical Solution Method for Fokker-Planck Equations with Application to Structural Reliability, *Probabilistic Engineering Mechanics*, Vol.6, No.1, p.33-48, 1991

[9] Spencer, B.F. and Bergman, L.A., On the numerical solution of the Fokker-Planck equation for nonlinear stochastic systems, *Nonlinear Dynamics*, Vol.4, No.4, p.357-372, 1993

[10] Naess, A. and Moe, V. Efficient path integration methods for nonlinear dynamic systems, *Probabilistic Engineering Mechanics*, Vol.15, No.2, p.221-231, 2000

[11] Yu, J.S. and Lin, Y.K., Numerical path integration of a non-homogeneous Markov process, *International Journal of Non-Linear Mechanics*, Vol.39, No.9, p.1493-1500, 2004

[12] Masud, A. and Bergman, L.A., Application of multi-scale finite element methods to the solution of the Fokker–Planck equation, *Computational Methods in Applied Mechanics and Engineering*, Vol.194, No.1, p.1513-1526, 2005

[13] Kazem, S., Rad, J.A. and Parand, K., Radial basis functions methods for solving Fokker-Planck equation, *Engineering Analysis with Boundary Elements*, Vol.36, No.2, p.181-189, 2012

[14] Dehghan, M. and Mohammadi, V. The numerical solution of FokkerPlanck equation with radial basis functions (RBFs) based on the meshless technique of Kansas approach and Galerkin method, *Engineering Analysis with Boundary Elements*, Vol. 47, p.38-63, 2014

[15] Sadrinezhad, A., Sett, K. and Hariharan, S.I., Efficient Solution Algorithms for the Fokker-Planck-Kolmogorov Equations in Probabilistic Elastoplasticity, 2015

[16] Griebel, M., Sparse grids and related approximation schemes for higher dimensional problems. *Foundations of Computational Mathematics (FoCM05)*, p.106-161, 2006

[17] Kavvas, M.L., Nonlinear Hydrologic Processes: Conservation Equations for Determining Their Means and Probability Distributions. *ASCE Journal of Hydrologic Engineering*, Vol.8, No.2, p.44-53, 2003

[18] Larsson, E. and Fornberg, B., A numerical study of some radial basis function based solution methods for elliptic {PDEs}, *Computers & Mathematics with Applications*, Vol.46, No.56, p.891-902, 2003

[19] Sarra, S.A., Integrated multiquadric radial basis function approximation methods, *Computers & Mathematics with Applications*, Vol.51, No.8, p.1283-1296, 2006

[20] Fornberg, B., Driscoll, T.A., Wright, G. and Charles, R., Observations on the behavior of radial basis function approximations near boundaries, *Computers & Mathematics with Applications*, Vol.43, No.3-5, p.473-490, 2002

[21] Fornberg, B., Larsson, E. and Flyer, N., Stable Computations with Gaussian Radial Basis Functions, *SIAM J. Sci. Comput.*, Vol.33, No.2, p.869-892, 2011

[22] Fasshauer, G.E. and McCourt, M.J., Stable Evaluation of Gaussian Radial Basis Function Interpolants, *SIAM J. Sci. Comput.*, Vol.34, No.2, p.737-762, 2012

[23] Fornberg, B. and Zuev, J., The Runge phenomenon and spatially variable shape parameters in RBF interpolation, *Computers & Mathematics with Applications*, Vol.54, No.3, p.379-398, 2007